frontiers | Frontiers in Earth Science

TYPE Original Research
PUBLISHED 07 January 2025
DOI 10.3389/feart.2024.1460386

OPEN ACCESS

EDITED BY
Ebrahim Fathi,
West Virginia University, United States

REVIEWED BY
Zhongbei Li,
University of Wollongong, Australia
Ikponmwosa Iyegbekedo,
West Virginia University, United States

*CORRESPONDENCE
Xi Zhang,
zx566285@163.com

RECEIVED 13 July 2024
ACCEPTED 27 November 2024
PUBLISHED 07 January 2025

CITATION
Zhang X, Ma Y, Hu M, Zhao A and Yang W (2025) Experimental study on the correlation between pore evolution characteristics and seepage flow of loaded lignite.
Front. Earth Sci. 12:1460386.
doi: 10.3389/feart.2024.1460386

Experimental study on the correlation between pore evolution characteristics and seepage flow of loaded lignite

Xi Zhang[1,2]*, Yankun Ma[1,2], Mingye Hu[1], Aohan Zhao[1,2] and Wenwang Yang[1,2]

[1]Safety Science and Engineering College, Anhui University of Science and Technology, Huai Nan, China, [2]Key Laboratory of Safe and Effective Coal Mining Ministry of Education, Huai Nan, China

The pressure on coal affects the pore fracture structure, altering the seepage characteristics of fluids such as gas or water. A special pseudo-triaxial loading nuclear magnetic gripper was used for uniaxial compression testing of the coal body. The T_2 map of the lignite was tested online, and MRI imaging was performed. The correlation between the pore fracture structure evolution and seepage characteristics of lignite was studied. The results show that (1) there are three stages, namely, compression, pore development, and post-peak failure, which promote the development and evolution of medium pore and macropores in lignite. (2) Under uniaxial compression, the permeability of the lignite sample shows a "V-shaped" trend, first decreasing and then increasing. When the axial pressure reaches approximately 3.0 MPa, the mutation of the MRI signal increases, and the enhancement of the MRI signal of the sample is due to the cumulative effect of mutation after aggregation. The aggregation of water image signals reflects the distribution area of pores that dominate seepage. (3) Under uniaxial compression, the pore change rate S_i slightly decreased. The pore change rate S_i of medium pores and macropores showed a positive correlation with axial pressure, which is consistent with the total pore change trend. The compressibility coefficient C_p of the porous pores (medium pores and macropores) and the permeability stress sensitivity coefficient C_f exhibited a linear correlation. The fractal dimension D_2 and D_3 values of pores in the medium and macropores scale range are close to 3, with the maximum value of D_2 being 2.971. This indicates significant fractal characteristics, suggesting that medium pores are the most developed in this scale range. Researches show that that the middle pore has a greater stress sensitivity and shows obvious fractal characteristics during the load failure. The compressibility of the large pore is correlated with the permeability sensitivity, These results show can help elucidate the influence of the pores fracture structure on the seepage evolution of lignite.

KEYWORDS

uniaxial compression, pore fissure, permeability, fractal feature, stress-seepage interaction

1 Introduction

Mining disturbance has a significant impact on the stress state and internal structure of deep coal bodies. This, in turn, accelerates the process of coal body damage and destruction (Zhang B. Y. et al., 2022; Chen et al., 2024; Wang et al., 2023; Wang L. et al., 2021). Additionally, the loading effect of stress intensifies coal deformation, alters permeability, and influences the seepage of gas or water (Liu et al., 2022; Gao et al., 2023; Yao et al., 2022). Scholars have conducted numerous studies on changes in coal permeability under various loads Zhu et al. (2021) conducted an experimental test on coal loading and unloading, observing a decrease in gas permeability during the initial stages. However, when the stress difference exceeded the coal sample yield strength, coal expansion and increased permeability occurred Liu (2019) conducted a study on the evolution of coal permeability under cyclic loads and revealed a negative correlation between the change in permeability during loading/unloading and changes in confining pressure (Xu et al., 2018) examined the damage-permeability aging characteristics of briquette samples under different mechanical paths, discovering varying degrees of damage expansion and permeability changes. The differential stress ratio was identified as the primary factor influencing the varying damage-permeability characteristics of loading and unloading coal Li et al. (2010) analyzed the evolution of coal sample permeability under bidirectional loading and unloading stress, highlighting that the maximum change rate occurred when a substantial number of internal fractures appeared near the peak value of the sample Jia et al. (2020) found that the permeability of raw coal samples varied significantly at low confining pressures and only slightly at high confining pressures. Conversely, briquette samples displayed nearly equal changes in permeability throughout the entire loading and unloading process Zhai et al. (2022) performed a damage-permeability test using a coal-rock adsorption-percolation-mechanical coupling characteristic tester and examined coal under different loading and unloading rates, ultimately determining the influence of such rates on permeability characteristics.

During the process of coal failure under loading, the pore fracture structure of the coal body undergoes significant changes (Liu et al., 2021; Zhang T. et al., 2022; Tang et al., 2023). To analyze the structural changes in the holes and cracks, nuclear magnetic resonance (NMR) analysis technology was used for the mechanical tests Zhou et al. (2021) conducted online tests of the T_2 spectrum and water content distribution of raw coal samples under different water injection pressures and found that macropores and microfractur4es accounted for more than 99% of the permeability during water injection Yin et al. (2023) conducted five groups of uniaxial compression tests on pressure water-impregnated coal samples with different initial damage levels. Pores and microcracks in the coal samples initiated and developed, while macrocracks expanded and the interparticle bonding force decreased (Li et al., 2019) used an NMR test system to study the evolution characteristics

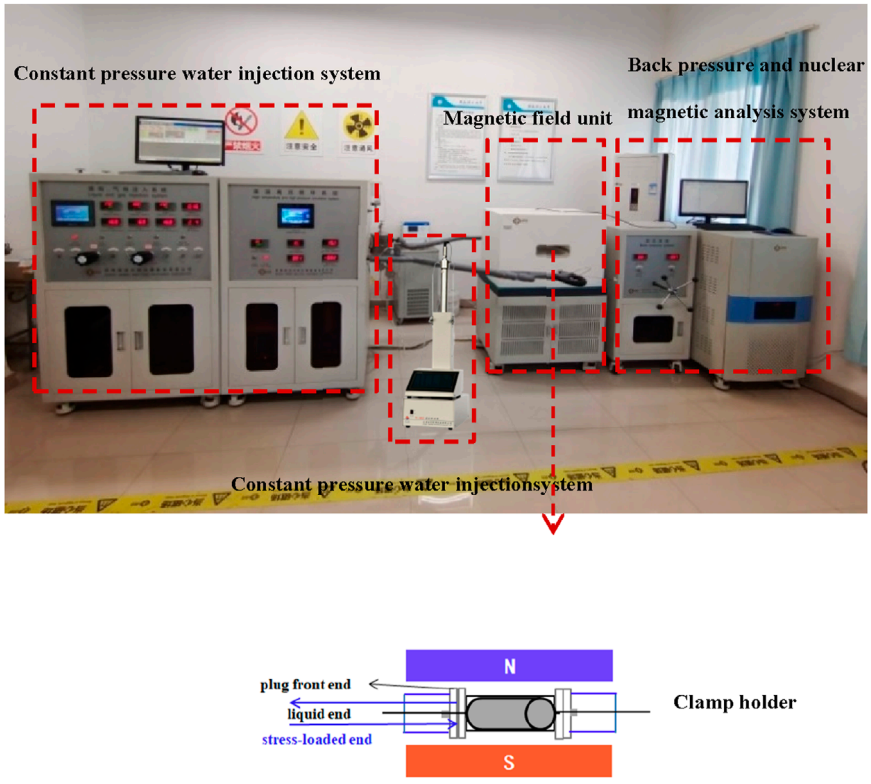

FIGURE 1
Schematic diagram of the seepage testing system under uniaxial compression.

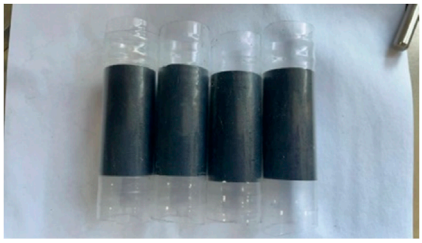

FIGURE 2
Lignite samples.

of pores and cracks in coal and rock under impact loading and discovered that the evolution of pores and cracks in coal under impact loading occurs through pore expansion, crack expansion, extension, and the generation of secondary cracks. Furthermore, the impact load enhances the connectivity between pores and cracks.

In that study of coal seepage Liu (2019), studied that the permeability of the different stratified coal samples is exponentially related to the maximum principal stress, the intermediate principal stress, the minimum principal stress and the effective stress. The initial permeability of the vertically stratified coal samples is only 13.5%, which is 22.2% of that for skewed bedding Fathi et al. (2012) studied that new double-slip Klinkenberg equation includes a characteristic length scale (L Ke) that is proportional to the kinetic energy per capillary cross-sectional area of the bouncing-back molecules by the capillary walls Ye et al. (2023) used the triaxials ervo-controlled seepage equipment for thethermo-fluid-solid coupling of coal containing. In the process of pore pressure loading,the permeability of coal firstly decreases rapidly and then tends to be flat, while the permeability of coal recovers when unloading,but it is smaller than the loading stage; under the same porepressure,the permeability of coal decreases with the increase of cycletimes.

Exploring the evolution and distribution law of the fine microstructure of coal and rock under loading can provide a reference and guidance for coal mine gas control and prevention of spontaneous coal seam combustion disasters in coal mine production. Therefore, a special pseudo-triaxial loading nuclear magnetic gripper was used to conduct uniaxial compression seepage tests on coal to explore the correlation between pore evolution characteristics and seepage during uniaxial compression.

2 Experimental system and scheme

2.1 Experimental system

The experimental system consisted of a low-field nuclear magnetic resonance experimental instrument, a special pseudo-triaxial loading nuclear magnetic clamp, a magnetic field unit, a constant pressure water injection system, an axial pressure control system (including a constant pressure and constant speed pump), and a back pressure and nuclear magnetic analysis system (Figure 1).

2.2 Test

Coal samples were selected from the Yihua coal in Xinjiang as depicted in Figure 2. Prior to the experiment, coals with good flatness and consistent bedding were chosen. The samples were the raw coal of Group B in Yihua, Xinjiang, and the coal recovered from the underground is polished into a 25mm × 50 mm cylindrical sample along the parallel bedding core. The physical parameters of the samples are listed in Table 1. The samples are lignite.

(1) Place the prepared lignite sample into the drying box and set the drying temperature to 70°C. Allow the sample to dry for 24 h to remove any water, and then allow it to naturally retain moisture for 12 h.
(2) Cover the lignite sample with a heat shrink tube and insert it into the gripper. Give a fixed confining pressure of 0.5 MPa. Set the experiment temperature to 25°C and connect the constant pressure and constant speed pump. The axial pressure control system for the coal sample experiment should start at 0 MPa, and increase the pressure loading by 0.5 MPa, until the coal sample is damaged.
(3) Connect the constant pressure water injection system and design the seepage liquid with an inlet end face pressure of 0.2 MPa, and an outlet pressure of 0.1 MPa. use the balance at the end of the gripper to record the water quality, the seepage test time, and calculate the flow rate.
(4) Replace the lignite sample and repeat steps 1–3.

TABLE 1 Industrial analysis parameters.

Lignite sample	Porosity (%)	Mad (%)	Aad (%)	Vad (%)	FC (%)
NO. 1	25.23	16.72	2.78	26.78	53.72
NO. 2	23.56				
NO. 3	22.94				
NO. 4	23.45				

Remark: Mad represents water content (%) of coal, Aad represents the ash content (%) of coal, Vad represents the amount of volatiles (%) of coal, and FC, represents the content of fixed carbon (%) of coal.

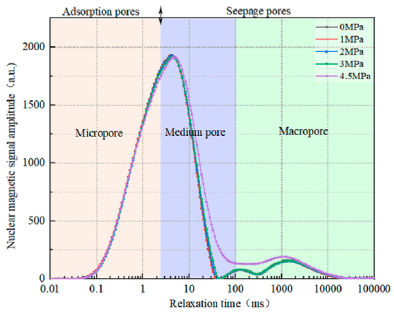

Lignite sample No.1-T_2 spectrum

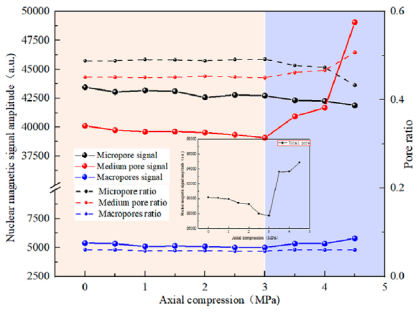

Pore volume change of lignite sample No.1

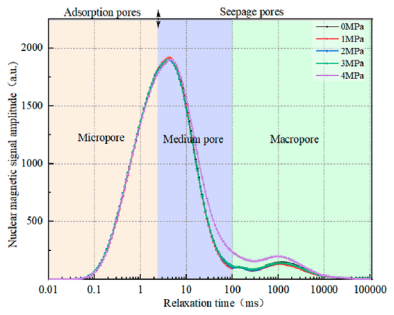

Lignite sample No.2-T_2 spectrum

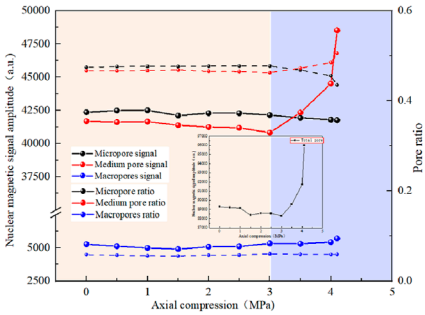

Pore volume change of lignite sample No.2

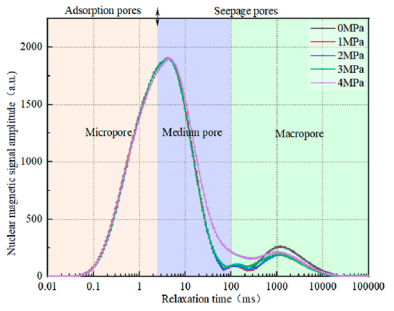

Lignite sample No.3-T_2 spectrum

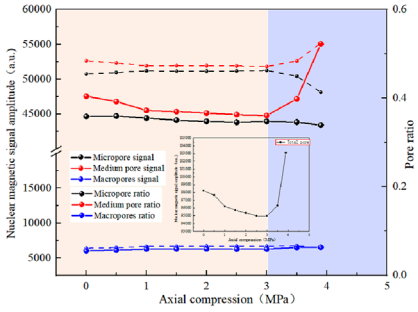

Pore volume change of lignite sample No.3

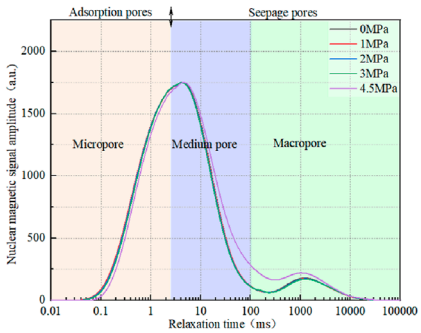

Lignite sample No.4-T2 spectrum

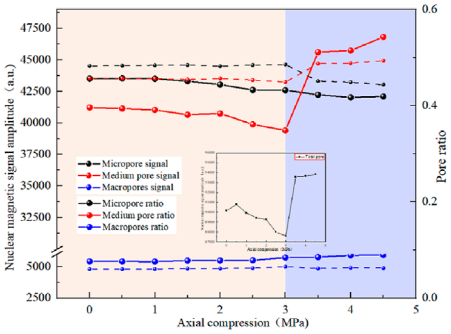

Pore volume change of lignite sample No.4

FIGURE 3
T_2 spectrum and pore volume changes under uniaxial compression. Lignite sample No. 3-T_2 spectrum. Pore volume change of lignite sample No. 3. Lignite sample No. 4-T2 spectrum. Pore volume change of lignite sample No. 4.

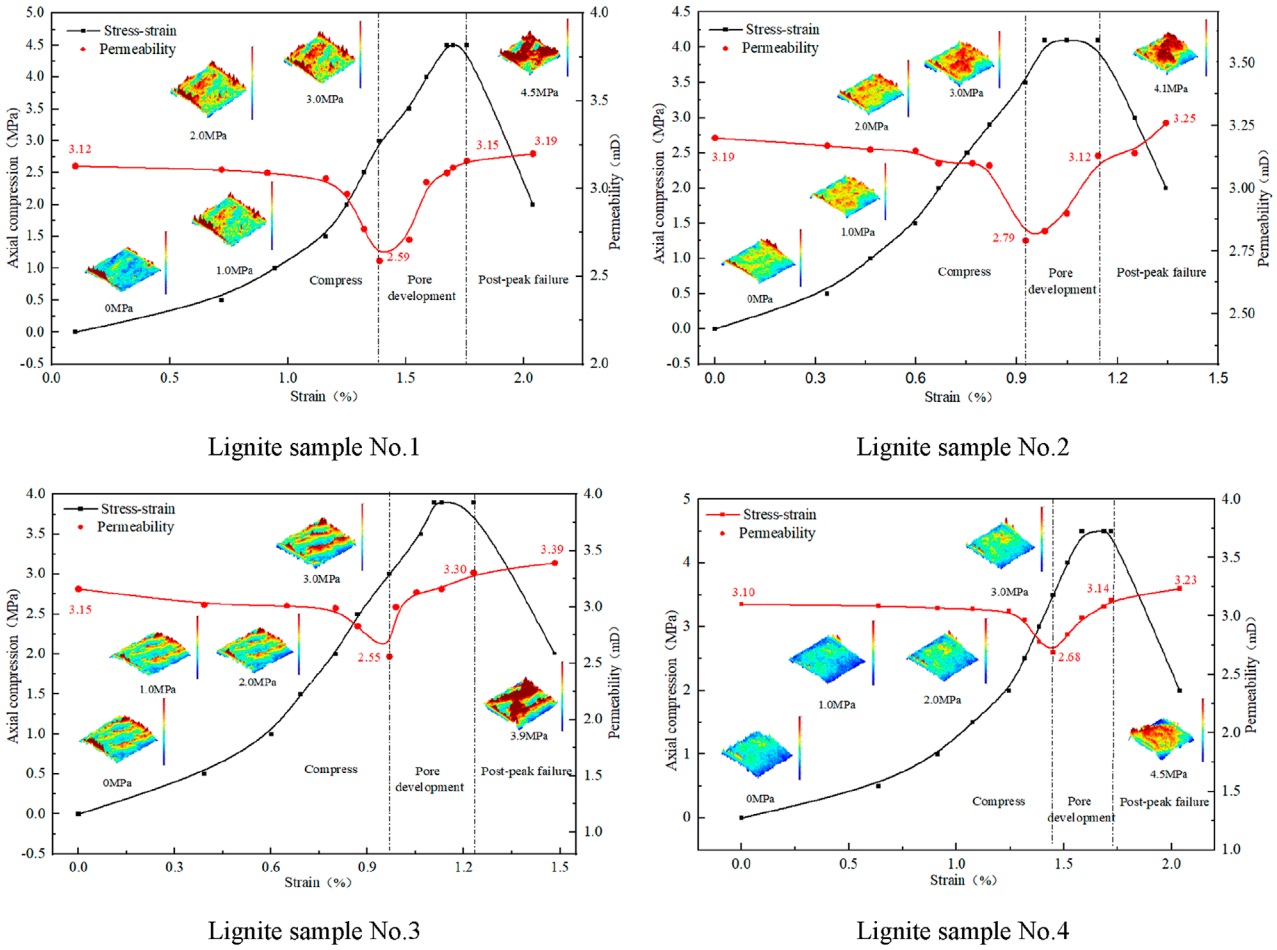

FIGURE 4
Stress-strain-permeability relationship diagram under uniaxial compression. Lignite sample No. 1. Lignite sample No. 2. Lignite sample No. 3. Lignite sample No. 4.

3 Results and discussion

3.1 Evolution characteristics of lignite pores and fractures under uniaxial compression

For the T_2 spectrum, the existing pore classification method categorizes the three peaks as micropores ($0 < T_2 < 2.5$ m), medium pores ($2.5\ m \leq T_2 < 100$ m), and macropores ($T_2 \geq 100$ m) (Tian et al., 2024; Xiong et al., 2022; Chao et al., 2022). Under uniaxial compression, lignite undergoes compression, pores development, and post-peak destruction. Experimental tests revealed that the T_2 spectrum and pore volume change diagram of lignite under uniaxial compression exhibit an increasing trend in the total pore signal, with no significant change in the T_2 spectrum of micropores (Li et al., 2020; Ren et al., 2017; Ren et al., 2022). However, the middle and macropores gradually connect with the axial compression load, resulting in an overall rightward shift in the T_2 spectrum. Micropores are commonly referred to as adsorption pores, whereas medium pores and macropores are collectively referred to as seepage pores.

Through T_2 spectrum analysis, the four coal samples, the pore peak areas of micropores decreased by 2.44%, 1.35%, 2.97%, and 9.23%, respectively, during loading from 0 MPa to failure. Conversely, the pore peak areas of medium pores increased by 17.61%, 19.56%, 14.14%, and 10.02%, respectively. Specifically, the pore peak areas of the macropores increased by 8.21%, 12.84%, 14.47%, and 7.25%, respectively. These results indicate that uniaxial compression promotes the development and evolution of porous pores, particularly medium pores and macropores. Initially, at the onset of pressure compression, the pore signal of the lignite body does not experience significant changes. However, as stress increases, the pore peak area of the medium pores rapidly increases when the lignite sample pressure reaches 80% of the peak stress, signifying the area of stress concentration pore evolution.

To analyze the contribution of various pores to lignite deformation, Ai and j represent the T_2 spectral area of pores in the i aperture range under J-axis compression, Aj represents the T_2 spectral area of total pores under J-axis compression, and Φi and j

TABLE 2 Values of C_p, C_f and ρ under uniaxial compression.

Axial compression (MPa)	Lignite sample No. 1			Lignite sample No. 2			Lignite sample No. 3			Lignite sample No. 4		
	C_p	C_f	ρ	C_p	C_f	ρ	C_p	C_f	ρ	C_p	C_f	ρ
0.5	0.3551	0.6351	1.0000	0.3543	0.6193	1.0000	0.3648	0.6050	1.0000	0.3563	0.6357	1.0000
1	0.1791	0.3155	1.0000	0.1775	0.3077	1.0000	0.1865	0.3015	1.0000	0.1787	0.3159	1.0000
1.5	0.1193	0.2083	0.9999	0.1193	0.2019	0.9999	0.1248	0.2004	0.9999	0.1199	0.2100	1.0000
2	0.0897	0.1516	0.9999	0.0894	0.1514	0.9999	0.0939	0.1498	0.9999	0.0897	0.1567	1.0000
2.5	0.0722	0.1131	0.9998	0.0716	0.1208	0.9999	0.0755	0.1134	0.9999	0.0732	0.1221	0.9999
3	0.0606	0.0882	0.9997	0.0598	0.0909	0.9998	0.0631	0.0855	0.9998	0.0613	0.0954	0.9998
3.5	0.0494	0.0791	0.9997	0.0496	0.0809	0.9998	0.0513	0.0896	0.9993	0.0460	0.0836	0.9997
4	0.0425	0.0807	0.9992	0.0414	0.0740	0.9997		—	—	—	—	—
3.9	—	—	—		—	—	0.0400	0.0872	0.9979	—	—	—
4.1	—	—	—	0.0371	0.0765	0.9992	—	—	—		—	—
4.5	0.0322	0.0726	0.9998	—	—	—	—	—	—	0.04003	0.0808	0.9993

represent the proportion of pores in the i aperture range under J-axis compression.

$$\Phi_{i,j} = A_{i,j}/A_j \quad (1)$$

Based on the pore volume change using Formula 1, the pore proportion of the lignite samples, as depicted in Figure 3, and the permeability variation under uniaxial compression, as shown in Figure 3, it can be concluded that the change in the pore proportion of the medium pores aligns with the trend of the total pore porosity. During the compression stage, the pore proportion of the four lignite samples decreases slowly, decreasing by 2.42%, 1.04%, 2.72%, and 2.70%, respectively. Conversely, the proportion of pores in medium holes rapidly increases until the failure of the lignite samples, with increases of 22.24%, 16.61%, 17.66%, and 15.57%, respectively. On the other hand, the proportion of small holes gradually decreases under pressure, decreasing by 7.61%, 11.37%, 6.42%, and 9.48%, respectively. These findings indicate that the stress sensitivity is greater for the medium pores than for the micropores.

3.2 Stress-seepage characteristics of lignite under uniaxial compression

In the process of uniaxial compression, the four lignite samples gradually experience failure under loading, with peak stresses of 4.5 MPa, 4.1 MPa, 3.9 MPa, and 4.5 MPa. Based on the permeability change observed during uniaxial compression and the MRI image (Figure 3), the permeability change trend of the lignite samples shows a "V" shape. When the stress loading reaches approximately 80% of the peak stress, the permeability decreases to its minimum value. Specifically, the permeability of lignite samples 1–4 decreases by 11.21%, 12.54%, 19.05%, and 13.54%, respectively. This indicates that the initial pressure applied to the lignite leads to compression deformation of the seepage hole, resulting in the closure of cracks, a reduction in effective seepage channels, and a significant decrease in permeability. In the pore development stage, the permeability of lignite samples 1-4 increases by 21.62%, 11.83%, 29.41%, and 17.16%, respectively. This increase suggests that friction and compression of the lignite matrix under axial pressure after lignite compaction produces a large number of connected porous pores (medium pores + macropores). With stress loading approaching the peak point, a substantial amount of water passes through these porous pores, resulting in a sudden increase in permeability. In the post-peak failure stage, the permeability of the four lignite samples exhibits continuous growth due to fracturing, increasing by 1.27%, 2.56%, 2.73%, and 2.87%, respectively.

During the uniaxial compression seepage process, MRI inversion imaging was performed on the four lignite bodies (Figure 4). The MR image shows regions with weak water signals in blue and regions with strong water signals in red. Darker colors indicate higher water content. In the early stage of compression, water diffuses axially through the top of the four lignite samples. However, the water signal in the axial direction of the lignite samples is not completely transmitted. When the axial pressure reaches approximately 3.0 MPa, the MRI signal of the samples is enhanced. This stage represents the development stage of pore cracks, indicating an increase in seepage pores (medium pores and macropores) and a notable enhancement of the MRI signal. The aggregation of water image signals reflects the development process and distribution area of vadose pores.

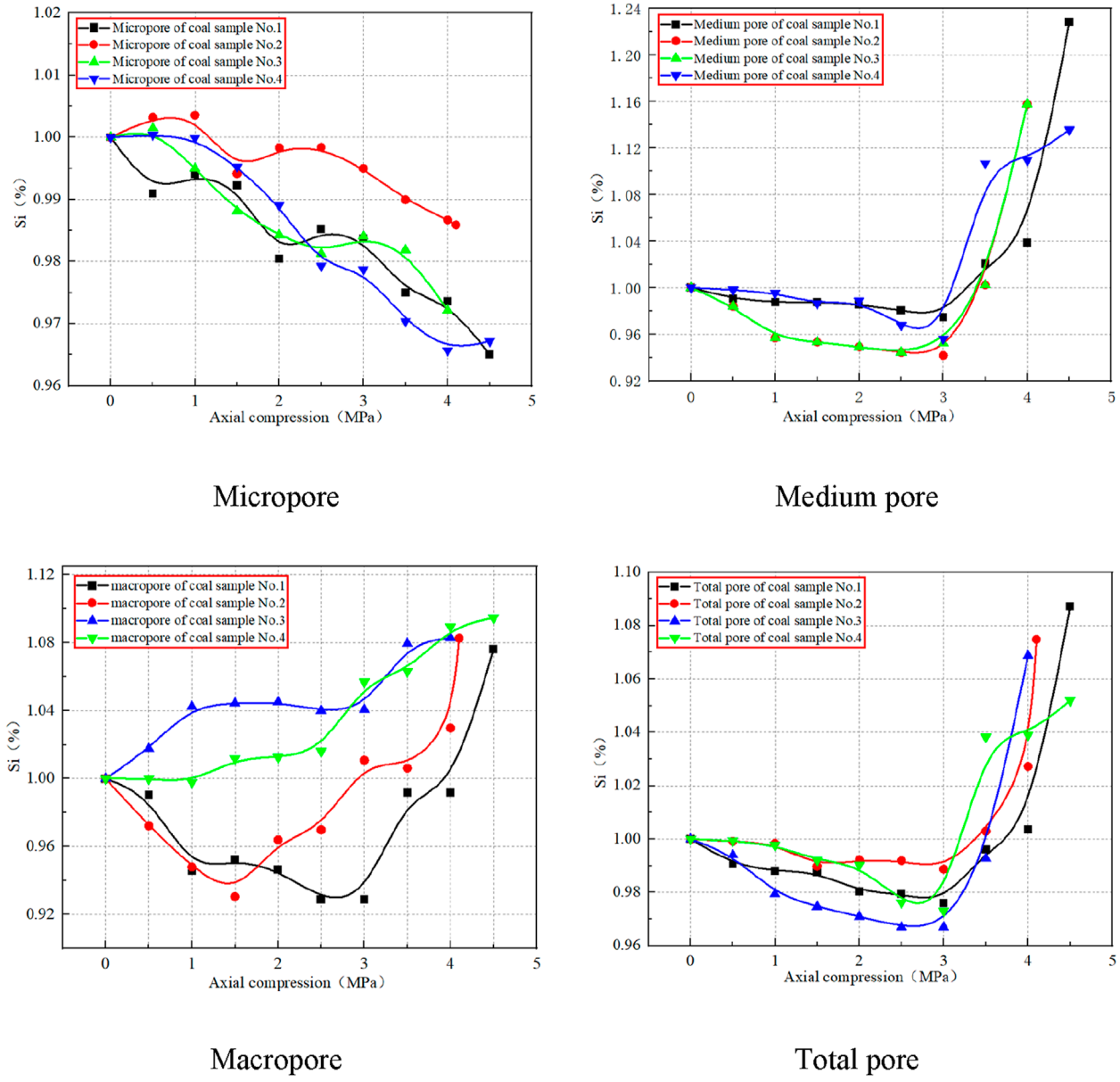

FIGURE 5
Pore change rate Si of lignite samples. Micropore, Medium pore, Macropore, Total pore.

3.3 Discussion on pore evolution and permeability correlations

To analyze the sensitive correlation between the evolution of different pore sizes and the permeability of lignite, the pore change rate and permeability change data under uniaxial compression were dimensionless. This analysis was conducted using Formulas 2, 4. The correlation between pore evolution and permeability was further discussed based on the formula for compressibility C_p (3) (Liu et al., 2016; David et al., 1994; Jiao et al., 2011), the permeability stress sensitivity coefficient C_f (5) (Wang M. L. et al., 2021; Liu X. G. et al., 2023; Liu H. H. et al., 2023), and the correlation degree Formula 6. The specific data can be found in Table 2, and the relationship diagram is depicted in Figure 5.

$$S_i = S_{i,j}/S_{i,0} \tag{2}$$

$S_{i,j}$ is the total pore area of aperture i (i represents micropores, medium pores and macropores); $S_{i,0}$ is the total pore area within the aperture range of i in the initial state.

$$C_p = \frac{1}{V_0}\frac{dv}{d\sigma} = \left(\frac{S_{i,j}}{S_{i,0}}\right)^{-1}/(\sigma-\sigma_0) \tag{3}$$

C_p is the coefficient of pore compressibility, V_0 is the pore volume, σ is the acting stress, and σ_0 is the initial stress.

$$\Delta K_i = K_i/K_0 \tag{4}$$

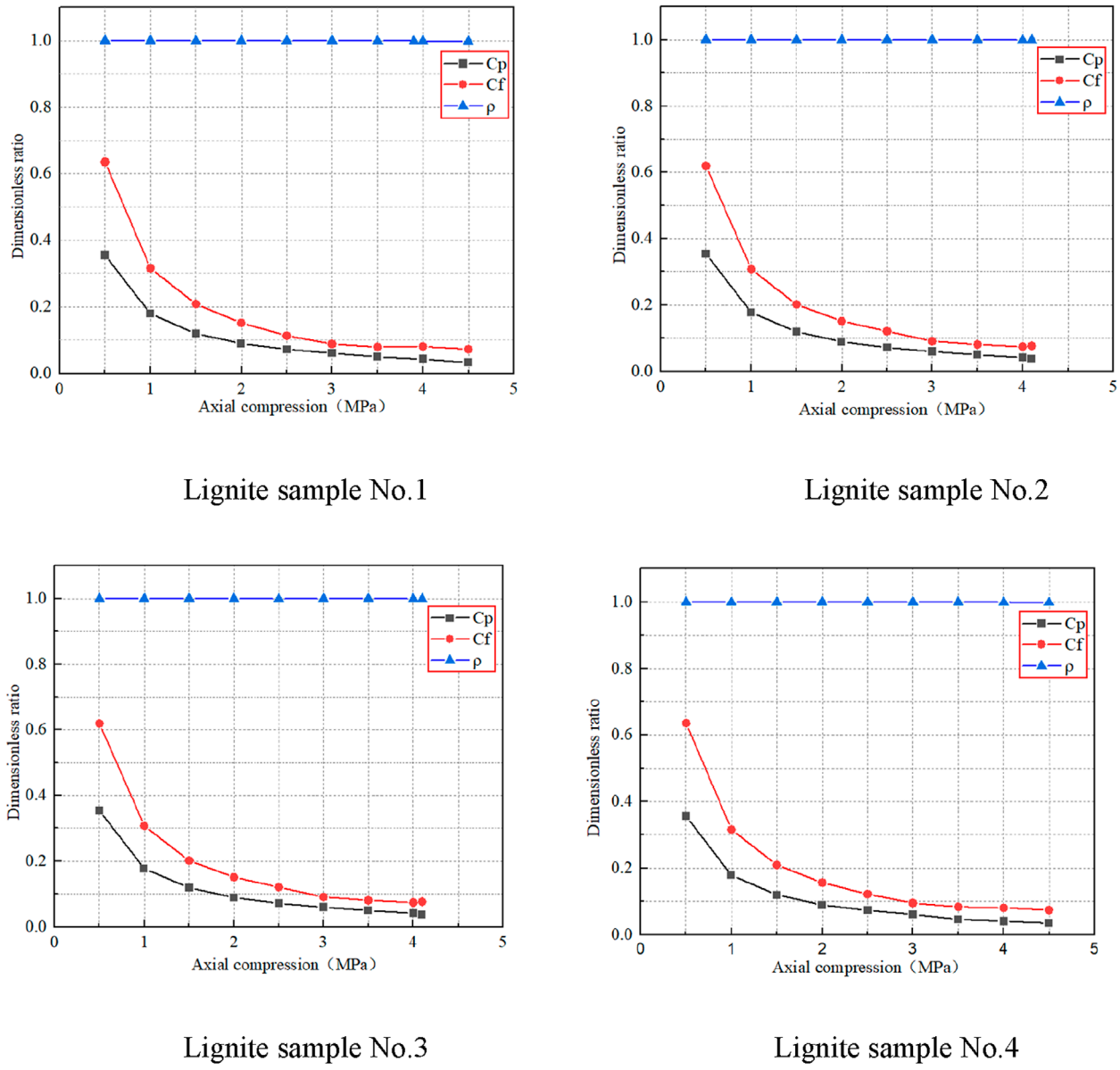

FIGURE 6
C_p, C_f and correlation diagram under uniaxial compression. No. 1. Lignite sample No. 2. Lignite sample No. 3. Lignite sample No. 4.

k_i represents the permeability of the coal sample under I-axial compression, and k_0 is the initial permeability.

$$C_f = \frac{\Delta K_i}{K_0} \frac{1}{\Delta \sigma_i} \tag{5}$$

C_f is the permeability stress sensitivity coefficient, and σ_0 is the stress variation.

$$\rho = \frac{Cov(x,y)}{\mu_x \mu_y} \tag{6}$$

Where Cov is the covariance of the two groups of data, μ is the variance, and x and y represent the dimensionless ratios of the pore change rate and permeability, respectively.

Under uniaxial compression, the pore change rate S_i of the lignite samples (Figure 5) exhibits certain characteristics. In the early stage of the axial compression loading process, the pore compression of small holes decreases due to stress. In the later stage of the axial compression loading process, the pore development and evolution result in a slight decrease in the pore change rate S_i of small holes. The reduction rates of pore S_i for the four coal samples are 3.43%, 1.37%, 2.71%, and 3.18%. In the early stage of axial compression loading, due to lignite body deformation, internal fracture closure, skeleton compaction, and extrusion, the pore change rate S_i of medium and macropores also slightly decreases. The decrease rates of medium pore S_i for the lignite coal samples are 2.42%、2.11%、4.79% and 4.41%. The decrease rates of macropore Si for the lignite coal samples are 8.88%, 2.11%、4.86% and 3.35%. However, when the

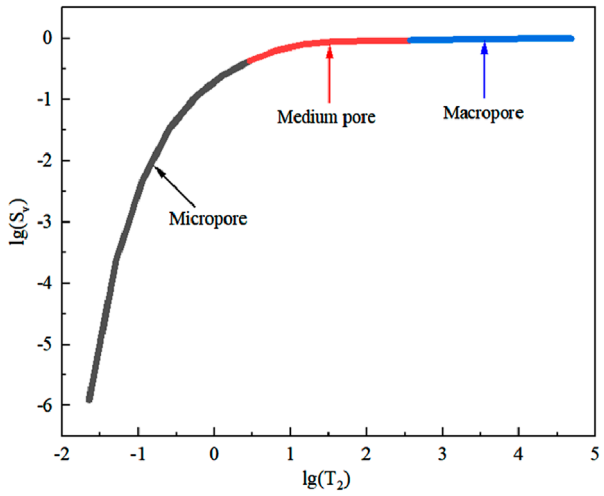

FIGURE 7
Value ranges of fractal dimensions of different pores.

axial compression loading is near 80% of the peak stress, the pore change rate S_i of the medium and macropores shows an increasing trend. The increase rates of medium S_i for the lignite coal samples are 26.14%, 18.09%, 21.25%, and 17.46%. The increase rates of Si in the macropores are 17.66%, 18.21%, 6.99%, and 10.72%, respectively. In summary, under uniaxial compression of lignite samples, the pore evolution is mainly characterized by slight decrease of medium and large pores and obvious increase of development in later period, which is consistent with the change trend of total pores. On the other hand, micropore S_i slightly decreases and negatively correlates with axial pressure. Therefore, the compressibility coefficient C_p and permeability stress sensitivity coefficient C_f of medium and macropores are selected to explore their correlation. This analysis was conducted using Formulas 3, 5 and 6.

The correlation between the compressibility coefficient C_p and permeability stress sensitivity coefficient C_r of the medium and macropores can be observed from this table and Figure 6. During uniaxial compression, the four samples exhibit strong linear correlations, with minimum coefficients ranging from 0.9983 to 0.9992. This indicates a significant relationship between these two factors. Furthermore, it is evident that changes in the volume of medium pores and macropores directly influence permeability.

3.4 Fractal characteristics of lignite pores under uniaxial compression

The fractal dimension (D) of the seepage space is correlated with the content of the seepage space (the peak area in the T_2 spectrum) and the separation coefficient of the coal samples (Yang et al., 2020; Li et al., 2023a; Li et al., 2023b). Within the effective range (approximately 3), a smaller D corresponds to a larger content of pore cracks in the seepage spaces of the lignite samples, a larger separation coefficient, and reduced heterogeneity. According to the equation $r = CT_2$, the nuclear magnetic resonance T_2 is directly proportional to the aperture r, and the cumulative volume fraction S_V with a radius less than r can be expressed as (Zhang and Weller, 2014; Wang X. J. et al., 2021; Zhang et al., 2018):

$$S_V = \frac{V(r)}{V_S} = \frac{r^{3-D} - r_{min}^{3-D}}{r_{max}^{3-D} - r_{min}^{3-D}} \tag{7}$$

The value of rmin is typically significantly smaller than that of rmax. As a result, Formula 7 can be simplified as follows:

$$S_V = \frac{r^{3-D}}{r_{max}^{3-D}} = \frac{T_2^{3-D}}{T_{2\,max}^{3-D}} \tag{8}$$

The logarithm is applied to both sides of the equation to derive an approximate fractal geometric formula for the NMR T2 spectrum.

$$\lg(S_v) = (3-D)\lg(T_2) + (D-3)\lg(T_{2\,max}) \tag{9}$$

$$\lg(S_v) = (3-D)\lg(T_2/T_{2\,max}) \tag{10}$$

The pore diameter corresponding to T_{2C} is taken as the dividing point to calculate the fractal dimension of the pore volume through the nuclear magnetic field test data. Based on the basic principle of fractal geometry, Used Formulas 8-10 to analyze and calculate, $0.03 \leq \lg T_2 < 0.46$ is selected as the value range of the small hole fractal, and $0.46 \leq \lg T_2 < 2.57$ is selected as the middle hole by deducing the theoretical formula of the T_2 spectrum. $\lg T_2 \geq 2.57$ is taken as the value range of the large hole (Figure 7), and S_V is calculated through the T_2 signal map. The fractal dimensions of the pore volume for small, medium, and large holes are called D_1, D_2, and D_3, respectively, and the relationship between the axial pressure and fractal dimension is obtained.

According to the data in Figure 3, the fractal dimension relationships of micropores, medium pores, and macropores under uniaxial compression are shown in Figure 8. D_1 of coal sample No. 1 ranges from 1.106 to 1.186, D_1 of coal sample No. 2 ranges from 1.057 to 1.156, D_1 of coal sample No. 3 ranges from 1.168 to 1.231, and D_1 of coal sample No. 4 ranges from 1.121 to 1.185 (Reference 2). The fractal dimension fitting correlation coefficient within the adsorption pore scale is low. The D2 values of the No. 1 lignite sample range from 2.966 to 2.970, those of the No. 2 lignite sample D_2 range from 2.961 to 2.963, those of the No. 3 lignite sample D_2 range from 2.960 to 2.964, and those of the No. 4 lignite sample D_2 range from 2.965 to 2.971. Lignite sample D_3 ranges from 2.618 to 2.642, No. 2 lignite sample D_3 ranges from 2.589 to 2.619, No. 3 lignite sample D_3 ranges from 2.618 to 2.644, and No. 4 lignite sample D_3 ranges from 2.623 to 2.642. In the uniaxial compression process, D_2 and D_3 both show a decreasing trend, and the values of D_2 and D_3 are close to 3, indicating that the pores in the porous pores (medium pores and macropores) of lignite have obvious fractal characteristics, in which D_2 is the largest and closest to 3, indicating that the medium pores are the most developed in the scale range.

We add image binary method to discuss the relationship between pore fractal and seepage. he fractal dimension of the binary graph under each stress path is calculated and analyzed, and the evolution law of the fractal dimension of the seepage channel is obtained. The decrease of fractal dimension of binary diagram indicates that the uniformity of seepage channel distribution in coal body decreases, while the increase of fractal dimension indicates that the uniformity of seepage channel distribution increases.

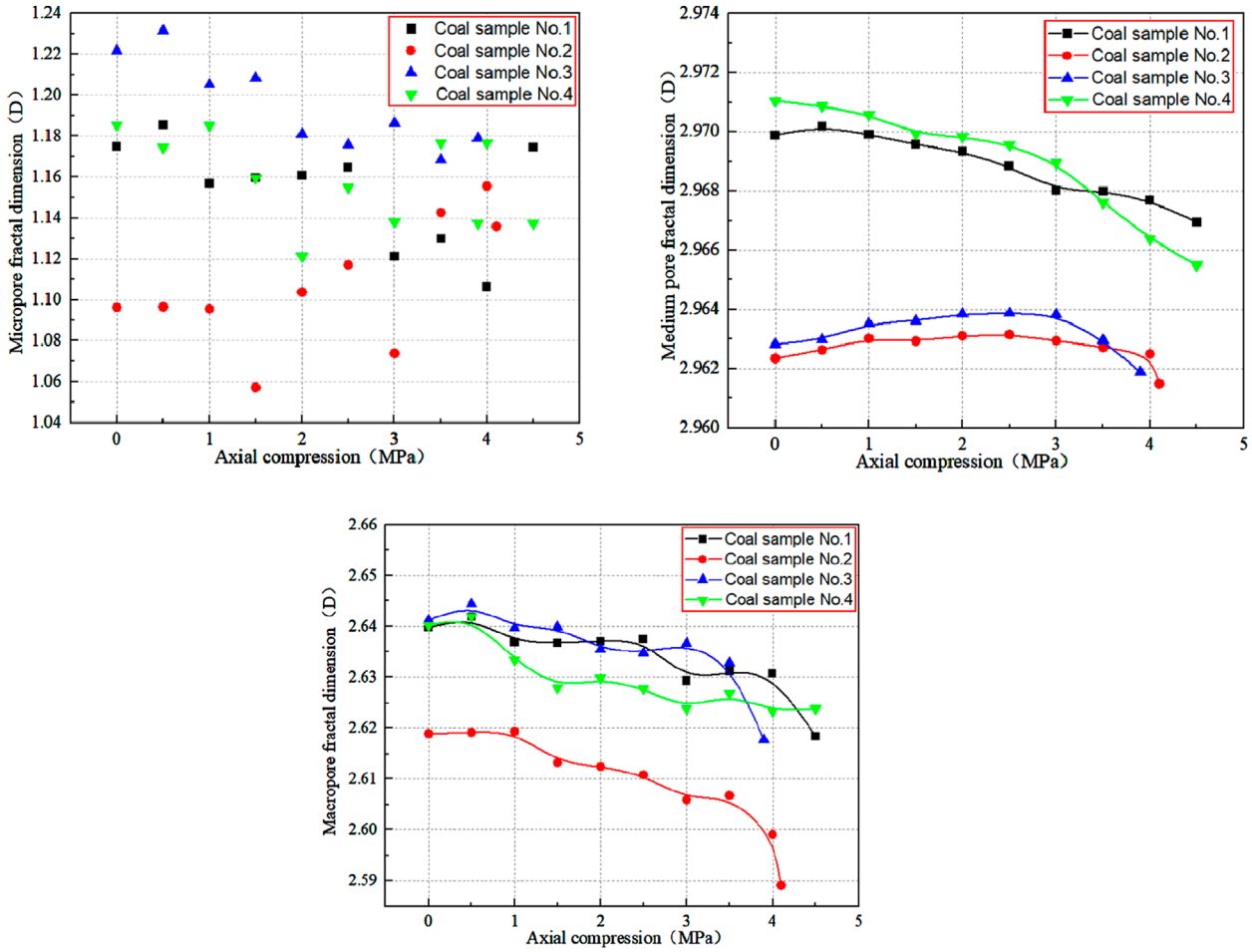

FIGURE 8
Fractal dimensions of micropore, medium pore and macropore under uniaxial compression.

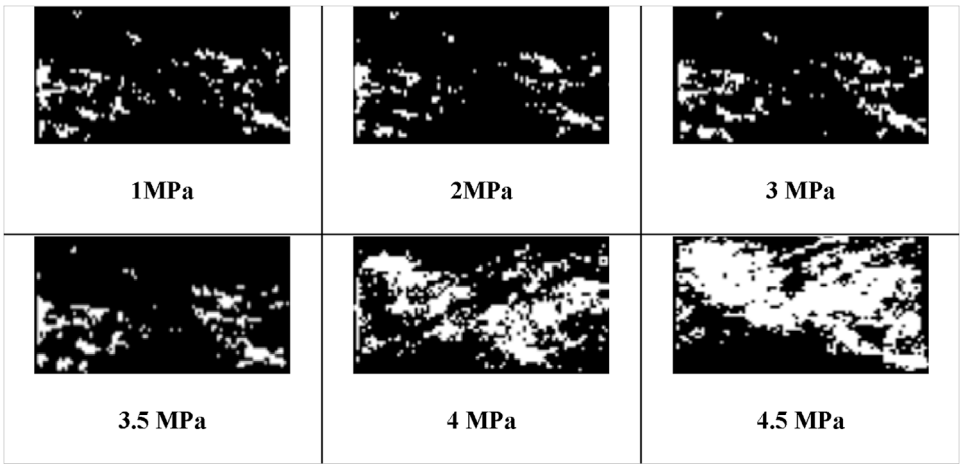

FIGURE 9
Binary diagram under stress.

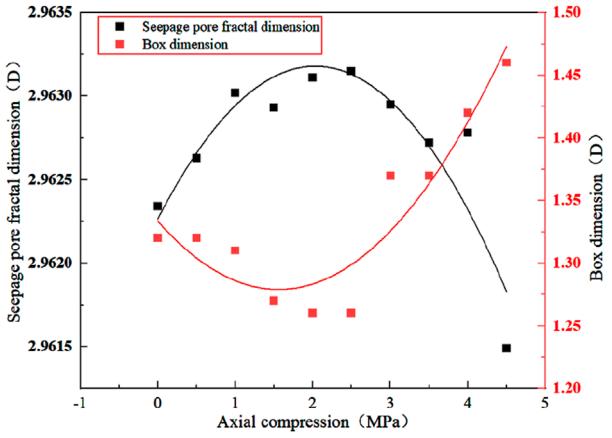

FIGURE 10
Dimension of seepage channel box in different loading stages of coal.

The gray MRI images obtained by the test were binarized by Matlab program, and the grid was divided. Figure 9 is based on the collection of white pixels formed by the high signal area in the MRI image, whose practical significance is the seepage channel inside lignite. One piece of sample is selected for analysis. In the early stage of loading, the original white pixels gradually disappear, and the regions are dispersed into points; in the late stage of loading, the pixels begin to increase, and the original points begin to connect with the new points to create a new white pixel region, and the final region is linked with the region to form a complete seepage channel.

Combined with the decreasing fractal dimension of the medium and large pores in the coal body, it indicates that the coal body is in the process of compression, and the seepage channel is not opened in the early stage, and the evolution of the seepage channel occurs only in the peak stress area close to 70%–80%. The change of fractal dimension is not linear reduction, but a cumulative process, just like the change of the pores in the coal body. In the early stage of loading, the change is small, and with the increase of stress, the seepage channel will be completely opened.

Combined with the calculation results of the fractal dimension of the seepage hole and the box dimension of the seepage channel, it is obtained (Figure 10). In the elastic deformation stage of the coal body before 3Mpa, the connection of the seepage hole is poor, and the fractal dimension of the seepage hole increases in the early stage of compression. After the plastic deformation, the micro-fracture of the coal body is generated, the seepage channel is generated, and the fractal dimension of the seepage hole is reduced. The change of the box dimension of the seepage channel indicates that the distribution of the seepage channel in the space is more evenly expanded.

4 Conclusion

By conducting online NMR tests on lignite samples under uniaxial loading, along with analyzing T_2 maps, online imaging, and permeability test data during lignite loading, we were able to quantitatively calculate the evolution law of pores and discuss the correlation between permeability and pore behavior. The following conclusions were drawn:

1) During the process of load failure in the lignite body, after three stages of compression, pore development, and post-peak failure, the change rate of pore signals in the four lignite samples was found to be minimal. However, the signals from medium pores and macropores demonstrated an increasing trend, with average increases of 18.02% and 8.72%, respectively. This indicates that uniaxial compression promotes the development and evolution of medium and macropores in the lignite body, with medium pores showing greater sensitivity to stress.
2) During the uniaxial compression process, the permeability of the lignite samples exhibited a “V-shaped” trend, initially decreasing and then increasing. In the early stage of compression, the axial water signals of the four lignite samples were not completely connected. However, when the axial pressure reached approximately 3.0 MPa, the MR signals of the samples were enhanced.
3) When subjected to uniaxial compression, the S_i in the pores slightly decreased and exhibited a negative correlation with the axial pressure. On the other hand, the change rate of the medium and macropores, S_i, exhibited a positive correlation with axial pressure, which is consistent with the overall trend observed in all the pores. The compressibility coefficient C_p of porous pores (medium pores and macropores) was found to be correlated with the permeability stress sensitivity coefficient C_f. The fractal dimensions D_2 and D_3 of pores in the range of medium pores and macropores in the lignite body were found to be close to 3, indicating the presence of significant fractal characteristics in this range. The maximum value of D_2 was determined to be 2.971, which is close to 3, suggesting that the medium pores are the most developed within this scale range.
4) Combined with the fractal dimension of seepage pore and seepage channel, it is obtained that in the uniaxial compression elastic deformation stage of coal body, the connectivity of seepage pore is poor, the fractal dimension of seepage pore increases, and the box dimension of flow channel decreases. When the coal body enters the plastic deformation stage, the coal body produces cracks, the seepage pore develops obviously, the fractal dimension of pore decreases, the box dimension of seepage channel increases, and the distribution space of seepage process is larger.

Data availability statement

The authors declare that all data, models or code generated or used during the research process can be obtained from the corresponding author on request.

Author contributions

XZ: Writing–original draft, Funding Acquisition, Formal Analysis, Software. YM: Supervision, Funding acquisition, Validation, Writing–review and editing. MH: Data curation, Writing–original draft, Validation and Methodology. AZ: Writing–original draft, Resources and Investigation. WY: Writing–review and editing, Visualization and Project Administration.

Funding

The author(s) declare that financial support was received for the research, authorship, and/or publication of this article. This study was supported by Natural Science Research Project of Anhui Universities, No. KJ2021A0419, National Natural Science Foundation of China, No. 52174161.

Conflict of interest

The authors declare that the research was conducted in the absence of any commercial or financial relationships that could be construed as a potential conflict of interest.

Publisher's note

All claims expressed in this article are solely those of the authors and do not necessarily represent those of their affiliated organizations, or those of the publisher, the editors and the reviewers. Any product that may be evaluated in this article, or claim that may be made by its manufacturer, is not guaranteed or endorsed by the publisher.

Supplementary material

The Supplementary Material for this article can be found online at: https://www.frontiersin.org/articles/10.3389/feart.2024.1460386/full#supplementary-material

References

Chao, L. W., Yu, Z., Lin, N., and Jing, B. (2022). Permeability evolution of coal subjected to triaxial compression based on *in-situ* nuclear magnetic resonance. *Int. J. Rock Mech. Min.*, 159. doi:10.1016/j.ijrmms.2022.105213

Chen, A. K., Cheng, Z., Xu, Y., Zheng, Y., Cong, Y., and Wu, J. (2024). Deformation and failure characteristics of strong–weak coupling structures with different height ratios under cyclic loading and unloading. *Acs. Omega* 9, 17076–17088. doi:10.1021/acsomega.3c08786

David, C., Wong, T. F., Zhu, W. L., and Zhang, J. (1994). Laboratory measurement of compaction-induced permeability change in porous rocks: implications for the generation and maintenance of pore pressure excess in the crust pore pressure excess in the crust. *Pure Appl. Geophys.* 143(13): 425–456. doi:10.1007/bf00874337

Fathi, T., Tinni, A., and Akkutlu, I. Y. (2012). Correction to Klinkenberg slip theory for gas flow in nano-capillaries. *Int. J. Coal Geo.* 103, 51–59. doi:10.1016/j.coal.2012.06.008

Gao, J. L., Wang, D. K., Guan, M. Y., and Zhang, C. (2023). Effect of acidification on different bedding of high-rank coal Study on the influence of directional antireflection effect. China. *Saf. Sci. J.* 33 (10), 46–52. doi:10.13637/j.issn.1009-6094.2022.2395

Jia, H. Y., Wang, K., Wang, Y. B., and Sun, X. K. (2020). Permeability characteristics of gas-bearing coal specimens under cyclic loading-unloading of confining pressure. *J. China Coal Soc.* 45 (5), 1710–1718. doi:10.13225/j.cnki.jccs.DY20.1112

Jiao, C. Y., He, S. L., and Xie, Q. (2011). An experimental study on stress dependent sensitivity of ultralow permeability sandstone reservoirs. *Acta Pet. Sin.* 32 (3), 489–494. doi:10.7623/syxb201103018

Li, D. Y., Wang, W., Li, H. M., Gao, B. B., and Su, C. D. (2010). Research on permeability of large-sized coal sample in loading and unloading test. *J. Min. and Saf. Eng.* 27 (1), 121–125.

Li, S., Wang, X. H., Fan, C. J., Zhang, H. H., Liu, Z., and Yin, K. (2019). Experimental study on evolution characteristics of coal pores under impact loadings. *China Saf. Sci. J.* 29(10) 91–97. doi:10.16265/j.cnki.issn1003-3033.2019.10.014

Li, Z., Liu, D., Cai, Y., Wang, Y., and Si, G. (2020). Evaluation of coal petrophysics incorporating fractal characteristics by mercury intrusion porosimetry and low-field NMR fractal characteristics by mercury intrusion porosimetry and low-field NMR. *Fuel* 263,116802. doi:10.1016/j.fuel.2019.116802

Li, Z. B., Ren, T., Li, X. C., Cheng, Y., He, X., Lin, J., et al. (2023a). Full-scale pore structure characterization of different rank coals and its impact on gas adsorption capacity: a theoretical model and experimental study. *Energy* 277, 127621–21. doi:10.1016/j.energy.2023.127621

Li, Z. B., Ren, T., Li, X. C., Qiao, M., Yang, X., Tan, L., et al. (2023b). Multi-scale pore fractal characteristics of differently ranked coal and its impact on gas adsorption. *Int. J. Min. Sci. Technol.* 33 (4), 389–401. doi:10.1016/j.ijmst.2022.12.006

Liu, D. M., Oiu, F., Liu, N., Cai, Y. D., Guo, Y. L., and Zhao, B. (2024). Pore structure characterization and its significance for gas adsorption in coals: a comprehensive review. *Processes* 18 (1821), 1–14.

Liu, X. G., Zhao, Y. Y., and Zhang, J. Q. (2023). Effect of nonlinear effective pressure on stress sensitivity in fracture sandstones J. *Sw Petrol Univ Sci and Tech* 45 (1), 127–135. doi:10.11885/j.issn.16745086.2020.12.0

Liu, H. H., Lin, B. Q., Jiang, C. B., Wang, Z. J., and Li, T. F. (2023). Sensitivity of coal permeability to multiple stresses. *J. Min. Saf. Eng.* 40 (4), 818–825. doi:10.13545/j.cnki.jmse.2022.0664

Liu, J. J., Gao, J. J., Zhang, X. B., Jia, G., and Wang, D. (2019). Experimental study of the seepage characteristics of loaded coal under true triaxial conditions. *Rock Mech Rock Eng.* 52 (2), 2815–2833. doi:10.1007/s00603-018-1720-x

Liu, T., Zhao, Y., and Lin, B. Q. Evolution of mechanical behavior and its influence on coal Permeability during dual unloading. *J. China Coal Soc.* 2022, 47(7): 2656–2667. doi:10.13225/j.cnki.jccs.2021.1179

Liu, Y., Zhang, T., Ma, Y. K., Yang, K., and Tang, M. (2021). Dynamic response and fractal characteristics of a pore-fracture system in ultralow permeability sandstone based on low-field NMR. *Energy and Fuels* 35 (1), 397–407. doi:10.1021/acs.energyfuels.0c03133

Liu, Y. Q. (2019). Experimental analysis of coal permeability evolution under cyclic loading. *J.China Coal Soc.* 44 (8), 2579–2588. doi:10.13225/j.cnki.jccs.2019.0353

Liu, Y. Q., Hou, J. L., Zhang, L., and Fan, S. W. (2016). Permeability experiments of pore structure in coal Matrix. *J. China Coal Soc.* 41 (2), 434–440. doi:10.13225/j.cnki.jccs.2016.0151

Ren, G. W. (2022). *The study on multiscale fractal characterization and permeability mechanism of pore structure in deep coal*. Beijing: China University of Mining and Technology. doi:10.27624/d.cnki.gzkbu.2022.000077

Ren, H. K., Wang, A. M., Li, C. F., Cao, D. Y., and Wei, Y. C. (2017). Study on pore characteristics of low-order coal reservoirs based on NMR technology. *Coal Sci. Technol.* 45(04) 143–148. doi:10.13199/j.cnki.cst.2017.04.025

Tang, M., Zhang, T., Ma, Y. K., Hao, D., Yang, X., and Li, Y. (2023). Experimental study on fracture effect on the multiphase flow in ultra-low permeability sandstone based on LF-NMR. *J. Pet. Sci. Eng.* 222, 211399. doi:10.1016/j.geoen.2022.211399

Wang, K., Guo, Y. Y., Wang, G., and Du, F. (2023). Seepage and mechanical damage charact-eristics of gas-containing complex coal rock mass under the true triaxial path. *J. China Coal Soc.* 48 (1), 226–237. doi:10.13225/j.cnki.jccs.ws22.0645

Wang, L., Liu, H. Q., Xie, G. X., Yuan, Q. P., and Chen, L. P. (2021). Fine characterization of gas structure structure gas gas-containing mechanism. Rock and Soil, *Mechanics* 42(12) 3203–3216. doi:10.16285/j.rsm.2021.1039

Wang, M. L., Gao, Y., and Yang, X. R. (2021). Field test of stress-sensitive effect in coalbed. *J. Exper. Mech.* 36 (6), 489–494.

Wang, X. J., Wang, M., Li, Y., Zhang, J., and Li, J. (2021). Shale pore connectivity and influencing factors based on spontaneous imbibition combined with a nuclear magnetic resonance experiment. *Mar. Petroleum Geol.* 179, 105239. doi:10.1016/j.marpetgeo.2021.105239

Xu, C., Fu, Q., Wang, K., Yuan, L., Zhang, X., and Wang, S. (2018). Effects of the loading methods on the damage-permeability aging characteristics of deep mining coal. *Min. Sci. Technol.* 47(1) 197–205. doi:10.13247/j.cnki.jcumt.000802

Yang, H., Cheng, W. M., and Liu, Z. (2020). Fractal characteristics of effective seepage channel structure of water infusion coal based on NMR experiment. *Rock Soil Mech.* 40 (4), 1–8. doi:10.16285/j.rsm.2019.0586

Yang, M., Liu, L., Zhang, X. B., Mao, J. R., and Chai, P. (2022). Nuclear magnetic resonance experimental study on pore structure and fluid characteristics of coal at different ranks. *Min. Saf. Environ. Prot.* 49 (01), 47–52.

Yao, C. H., Li, B. B., Gao, Z., Li, J. H., and Xu, J. (2022). Study on dual pore permeability model of coal under the conditions of pore pressure increasing and decreasing. *Coal Sci. Technol.* 50 (11), 116–121. doi:10.13199/j.cnki.cst.2021-0151

Ye, P. P., Li, B. B., Wu, X. H., Song, H. S., Chen, Q. Y., and Li, J. (2023). *Study on coal seepage evolution mechanism under cyclic loading and unloading*

of pore pressure. J. China University of Mining and Technology. 52 (4), 739–749.

Yin, D. W., Ding, Y. S., Wang, F., Jiang, N., Liu, H. M., and Tan, Y. (2023). Experimental study on mechanical properties of coal soaked in pressurized water considering initial damage. *J. China Coal Soc.* 48 (12), 4417–4432. doi:10.13225/j.cnki.jccs.2023.0256

Zhai, C., Sun, Y., Fan, Y. R., Yang, P. Q., Ge, X. M., and Wu, F. (2022). Application and prospect of low-field nuclear magnetic resonance technology in accurate characterization of coal pore structure. *J. China Coal Soc.* 47 828–848. doi:10.13225/j.cnki.jccs.xr21.1766

Zhang, B. Y., Yu, Y., Gao, X., Wu, Q., Zhang, X. H., and Zhang, Q. (2022). Permeability of mine gas hydrate bonded coal against loading-unloading of axial stress. *Chin. J. Rock Mech. Eng.* 41 (11), 2283–2298. doi:10.13722/j.cnki.jrme.2022.0063

Zhang, T., Tang, M., Ma, Y. K., Zhu, G., Zhang, Q., Wu, J., et al. (2022). Experimental study on CO_2/water flooding mechanism and oil recovery in ultralow permeability sandstone with online LF-NMR. *Energy* 252, 123948. doi:10.1016/j.energy.2022.123948

Zhang, P., Lu, S., Li, J., Chen, C., Xue, H., and Zhang, J. (2018). Petrophysical characterization of oil-bearing shales by low-field nuclear magnetic resonance (NMR). *Mar. Pet. Geol.* 89 (3), 775–785. doi:10.1016/j.marpetgeo.2017.11.015

Zhang, Z. Y., and Weller, A. (2014). Fractal dimension of pore-space geometry of an eocene sandstone formation. *Geophysics* 79(6) 77–87. doi:10.1190/geo2014-0143.1

Zhou, H. W., Liu, Z. L., Sun, X. T., Ren, W. G., Zhong, J. C., and Zhao, J. W. (2021). Evolution characteristics of seepage channel during water infusion in deep coal samples. *J. China Coal Soc.* 46(3) 686–696. doi:10.13225/j.cnki.jccs.yt20.1966

Zhu, J., Wang, Q., Tang, J., Chen, J. Y., Jiang, Y. D., Tang, D., et al. (2021). Evolution characteristics of strain and permeability of coal samples under loading and unloading conditions. *J. China Coal Soc.* 46 (4), 1203–1210. doi:10.13225/j.cnki.jccs.dy20.0280